Full Paper

Wiley Online Library

ELECTROANALYSIS

Special Issue GRAPHENE

DOI: 10.1002/elan.201300321

Study on Oxidation State Dependent Electrocatalytic Ability for I^-/I_3^- Redox Reaction of Reduced Graphene Oxides

Min-Hsin Yeh,[a] Lu-Yin Lin,[a] Tzu-Yen Huang,[a, b] Hui-Min Chuang,[a] Chih-Wei Chu,[b, c] and Kuo-Chuan Ho*[a, d]

Abstract: The influence of oxidation states on electrocatalytic abilities for I_3^- reduction is discussed for reduced graphene oxide (rGO), which is a promising catalyst of counter electrodes for dye-sensitized solar cells (DSSCs). The oxidation states of rGO can be controlled via a photothermal reduction process by varying exposure times. The results reveal that the rGO with lower oxidation state shows smaller charge transfer resistance at the electrode/electrolyte interface and better electrocatalytic ability attributed to higher standard heterogeneous rate constant (k^0) and reasonable electrochemical surface area (A_e) for I_3^- reduction, both are quantitatively determined by a rotating disk electrode system using the Koutecký–Levich equation.

Keywords: Counter electrode · Dye-sensitized solar cells · Electrocatalytic ability · Photothermal reduction process · Reduced graphene oxide

1 Introduction

Carbonaceous materials, such as graphite, diamond, fullerene, amorphous carbon, active carbon, carbon black (CB), carbon nanotubes (CNT), and graphene (GN) were widely studied in different fields, owing to the fact that the physical and chemical properties of carbon vary greatly with its form. Some allotropic forms of carbon attract a lot of attention for electrochemical applications, such as fuel cells [1], lithium-ions batteries [2], hydrogen storages [3], sensors [4], and supercapacitors [5], owing to their outstanding electrical conductivity, chemical durability, and electrocatalytic ability. These materials possess a high potential to replace expensive materials and thereby reducing the cost of the pertinent devices and also enhancing the performance and durability of such devices.

A counter electrode (CE) in a dye-sensitized solar cell (DSSC) has the roles of collecting electrons from the photoanode and reducing the triiodide ions (I_3^-) to iodide (I^-) in the electrolyte. Typically, a conducting glass with Pt catalytic layer is used as the CE of a DSSC, due to its outstanding electrocatalytic activity for I_3^- reduction, excellent electronic conductivity, and good chemical durability [6]. The Pt-coated conducting glass, which can be fabricated by various methods, e.g., thermal decomposition [7], sputtering [6,8], electrochemical deposition [9], chemical deposition [10], electroless deposition [11], is most commonly used CEs in DSSCs. However, the high cost of Pt is an issue to be considered for cost-effective fabrication of DSSCs, although it shows a high catalytic activity for I_3^- reduction and an excellent electronic conductivity. Replacement of Pt with other cheaper materials is required for reducing the production cost of the cells, especially when the production is in mass scale. Several carbonaceous materials, e.g., activated carbon [12], CB [13], acetylene-black spheres [14], hard carbon spherule [15], graphite [16], and multiwalled carbon nanotube (MWCNT) or single-walled carbon nanotube (SWCNT) [17] have become potential materials to substitute Pt, because of their low cost, high conductivity, and good catalytic ability for the reduction of I_3^-. Recently, Wu et al. proposed nine kinds of carbonaceous materials as the catalysts of CEs for DSSCs [18]. Murakami et al. employed CB as the catalyst for I_3^- reduction on a conducting glass for DSSCs and found the charge-transfer resistance for the thicker carbon layer is about one-third that of the Pt layer [13].

Ever since Novoselov and Geim have discovered the Noble Prize winning two dimensional GN in 2004 [19], it has been introduced in various electrochemical devices, such as sensors [20], lithium-ion batteries [21], and capac-

[a] M.-H. Yeh, L.-Y. Lin, T.-Y. Huang, H.-M. Chuang, K.-C. Ho
Department of Chemical Engineering, National Taiwan University, Taipei 10617, Taiwan
*e-mail: kcho@ntu.edu.tw

[b] T.-Y. Huang, C.-W. Chu
Research Center for Applied Sciences, Academia Sinica, Taipei 11529, Taiwan

[c] C.-W. Chu
Department of Photonics, National Chiao Tung University, Hsinchu 30010, Taiwan

[d] K.-C. Ho
Institute of Polymer Science and Engineering, National Taiwan University, Taipei 10617, Taiwan

Supporting Information for this article is available on the WWW under http://dx.doi.org/10.1002/elan.201300321.

itors [22], owing to its remarkable electrical, optical, thermal, and mechanical properties as well as its extraordinarily high surface area (~2,630 $m^2 g^{-1}$) [23]. Encouraged by these attractive properties of GN, some researchers have proposed it as the catalytic film on the CEs of DSSCs [24]. Based on these literatures, reduced graphene oxide (rGO), the most common GN-based material for use in the CEs of DSSCs, can be prepared by Hummers' method for producing the graphene oxide (GO) sheets and further reducing by thermal reduction or chemical reduction method [25]. Therefore, effective reduction process for fabricating the rGO and good understanding on the role of oxidation state of rGO are critical issues for developing rGO-based CE for DSSCs. Chien et al. had demonstrated that the photoluminescence property of rGO can be easily controlled by photothermal reduction process at various exposure times [26]. Therefore, it is reasonable to presume that the performance of rGO for reducing the I_3^- may be influenced by different oxidation states.

In this study, GO was prepared by a modified Hummers' method from graphite powder and further reduced to rGO by applying a photothermal reduction process. The morphologies and characteristics of graphite powder and as-prepared GO were observed using transmission electron microscopy (TEM) and Raman spectra. The oxidation states of rGO with various exposure times of the photothermal reduction process were confirmed by Raman spectra and contact angle analysis. The electrode containing rGO at high exposure time (72 h) not only shows better electrocatalytic ability of its CE for the reduction of I_3^- but also gives a smaller charge transfer resistance at the electrode/electrolyte interface, as revealed by cyclic voltammetry (CV), electrochemical impedance spectra (EIS), and Tafel polarization analyses. Furthermore, the realistic electroactive surface area (A_e) and the standard heterogeneous rate constant (k^0) for I_3^- reduction reaction were quantitatively determined by a rotating disk electrode (RDE) system using Koutecký–Levich equation. The results of RDE conclude that the better electrocatalytic ability of rGO with high exposure time (72 h) is not only caused by its higher k^0 for I_3^- reduction reaction, but also by its resonable A_e to provide active sites for reducing I_3^-. This study aims at quantifying the electrocatalytic ability for the reduction of I_3^- on the rGO with various oxidation states.

2 Experimental

2.1 Materials

Lithium iodide (LiI, synthetical grade), iodine (I_2, synthetical grade), and potassium permanganate ($KMnO_4$, 98%) were obtained from Merck. Guanidinium thiocyanate (GuSCN, 99%), 4-*tert*-butylpyridine (tBP, 96%), sodium nitrate ($NaNO_3$, 99%), sulfuric acid (H_2SO_4, 95%) and *tert*-butyl alcohol (tBA, 96%) were obtained from Acros. Graphite powder (SP-1, 99.99%) was obtained from Bay Carbon Inc. Hydrogen peroxide (H_2O_2, ~30%), lithium perchlorate ($LiClO_4$, ≥98.0%), tetrabutylammonium triiodide ($TBAI_3$, >97%), and Nafion 117 solution (~5% in a mixture of lower aliphatic alcohols and water) were obtained from Sigma–Aldrich. Acetonitrile (ACN, 99.99%) was obtained from J. T. Baker. 3-Methoxypropionitrile (MPN, 99%) was obtained from Fluka. 1,2-Dimethyl-3-propylimidazolium iodide (DMPII) was obtained from Solaronix (S. A., Aubonne, Switzerland). A tin-doped In_2O_3 (ITO, UR–ITO007–0.7 mm, 10 Ω $sq.^{-1}$, Uni-onward Corp., Taipei, Taiwan) conducting glasses were first cleaned with a neutral cleaner and then washed with deionized water, acetone, and IPA sequentially. Pt-coated electrode was prepared by sputtering (film thickness ~50 nm) on the ITO substrate.

2.2 Preparation of GO and rGO with Various Oxidation States

GO was prepared from graphite powder using a modified version of Hummers' method [27]. Briefly, graphite powder (2 g), $NaNO_3$ (1 g), and H_2SO_4 (46 mL) were mixed in an ice bath and then $KMnO_4$ (6 g) was added slowly. Once mixed, the solution was transferred to a water bath and stirred at 35 °C for approximately 1 h, forming a thick paste. Deionized water (80 mL) was added and then the solution was stirred for 1 h at 90 °C. Finally, more deionized water (200 mL) was added, followed by the slow addition of H_2O_2 (30%, 6 mL). The warm solution was filtered and washed sequentially with 10% HCl (200 mL) for three times and deionized water (200 mL) for one time. The filter cake was dispersed in water through mechanical agitation and then stirred overnight. The dispersion was left to settle and the supernatant (clear yellow dispersion) was subjected to dialysis for 1 month, resulting in a stock solution having a GO concentration of approximately 0.17 mg mL^{-1}. The stable dispersion was filtered through an alumina membrane (Anopore, Pore size = 0.2 μm, Whatman, UK) and left to dry for several days. The GO paper was then carefully peeled from the filter and stored under ambient conditions.

The rGO with various oxidation states were controlled by applying modified photothermal reduction with various exposure times [26]. Briefly, aqueous GO solution (2 mg mL^{-1}) was prepared and subjected to steady-state Xe lamp irradiation (250 W) with different exposure times (6–72 h). Based on our experiment results, the oxidation state of rGO cannot be further altered by increasing the exposure time longer than 72 h (data not shown). Hence, the maximum exposure time is fixed at 72 h in this work. Photothermal reduction provides a gradual transformation from GO to rGO, this implies that the oxidation state of rGO can be controlled by the exposure time. The electrocatalytic ability of rGO with various oxidation states for reducing I_3^- can be explored systematically.

2.3 Characterization of GO and rGO with Various Oxidation States

Aqueous solutions with 2 wt% of GO and rGO under various exposure times (6–72 h) were used for depositing the corresponding films on the ITO glasses, by drop coating technique. The structure of graphite powder and GO were investigated by transmission electron microscopy (TEM, JEM–1230, JEOL, Tokyo, Japan). UV-visible spectrophotometer (UV-vis, V-570, Jasco Inc., Maryland, USA) was used to investigate the color change from GO to rGO in aqueous solutions. The degrees of defects of the GO and rGO under various exposure times were estimated by Raman spectra, using a Dimension Raman system with 532 nm laser source (P2, Lambda Solution, Inc., USA). The contact angles of the films with GO and rGO under various exposure times on the ITO substrate were measured using a contact angle system (FTA125, First Ten Angstroms, Inc., Portsmouth, UK).

2.4 Electrochemical Measurements for GO and rGO with Various Oxidation States

CV was performed to investigate electrocatalytic abilities of the electrodes with GO and rGO under various exposure times. The CV was carried out in a three-electrode electrochemical system, by using either GO or rGO prepared under various exposure times as the working electrode, Pt foil as the counter electrode, and an Ag/Ag^+ electrode as the reference electrode in an ACN solution, containing 10.0 mM I^-, 1.0 mM I_2, and 0.1 M $LiClO_4$.

A symmetric cell was used to investigate the electrocatalytic abilities for both GO and rGO, via EIS, applying a frequency range from 10 mHz to 100 kHz [28]. The cell consisted of an iodide/triiodide (I^-/I_3^-) electrolyte, precisely 0.1 M LiI, 0.6 M DMPII, 0.05 M I_2, and 0.5 M tBP in MPN/ACN (volume ratio = 1:1), and two identical electrodes each with an area of 1 cm^2, separated by a Surlyn spacer film of 60 μm thick. Impedance spectroscopic data were obtained, optimized by fitting to an equivalent circuit, using Z-View software [29].

Tafel polarization curves were obtained with the same symmetric cell by using an electrochemical potentiostat (scan rate: 100 $mV\,s^{-1}$). The exchange current density (J_0) of an electrode, which can be obtained from the Tafel zone, is tantamount to the electrocatalytic ability of the electrode [30]. The value of J_0 can be estimated from the extrapolated intercepts of the anodic and cathodic branches of the corresponding Tafel curves at the current density axes.

Intrinsic heterogeneous rate constant (k^0) and effective electroactive surface area (A_e) for the reduction reaction of I_3^- on GO and rGO under various exposure times were quantitatively determined by a RDE system as mentioned above, by using the Koutecký-Levich equation. The RDE system was equipped with a modulated speed rotator (PINE Instrument Company) and was connected to a potentiostat (model 900B, CH Instruments, Texas, USA). GCEs (working area: 0.247 cm^2, Part #AFE7R9GCGC, PINE Instrument Company) were deposited with thin films of GO or rGO under various exposure times by drop coating (15 μL, 30 μg catalyst); the electrodes were dried at ambient temperature. The GCEs coated with these films had served as the working electrode, Pt foil as the counter electrode, and an Ag/Ag^+ as the reference electrode. The electrolyte used was an ACN based solution, containing 0.1 M $LiClO_4$ and 1.0 mM $TBAI_3$. CV curves were obtained by scanning the potential of the working electrode from −0.8 to 1.0 V (vs. Ag/Ag^+) at a scan rate of 50 $mV\,s^{-1}$ (in absence of rotation). Five linear sweep voltammetric (LSV) curves (not shown) were acquired for the above electrode by controlling the rotating speed (50, 100, 200, 400, 600, and 800 rpm), at a scan rate of 1 $mV\,s^{-1}$ (scan range: 0.1 to −0.6 V vs. Ag/Ag^+). A corresponding current, i, could be obtained from each of the LSV curves at the formal potential (E_0). Thus, plots of i^{-1} vs. $\omega^{-1/2}$ were made for the GCE coated with the films of GO or rGO under various exposure times.

3 Results and Discussion

3.1 Morphologies and Characteristics of As-Prepared GO

Transmission electron microscopy (TEM) images of the graphite powder and as-prepared GO are shown in Supporting Information Figure S1a and b, respectively. Graphite powder shows a dense-planar structure with several stacked layers, and GO possesses a planar sheet structure, like ultra-thin paper, with several monolayers stacked together. Figure S1c presents the Raman spectra of graphite powder and as-prepared GO, containing D band (1355 cm^{-1}, ring breathing mode from sp^2 carbon rings, A_{1g} mode) and G band (1579 cm^{-1}, planar configuration sp^2 bonded carbon with bond-stretching motion, E_{2g} mode). Raman spectra show higher ratio of D peak intensity to G peak intensity (I_D/I_G) for the as-prepared GO than that for graphite powder, implying the successful exfoliation of graphite powder to form GO [31].

3.2 Oxidation States of GO and rGO Under Various Exposure Times of Photothermal Reduction: Raman Spectra and Contact Angle Analysis

GO was further reduced to rGO by a photothermal reduction process [26]. Figure 1 displays the normalized absorbance spectra of GO and rGO obtained after a photothermal reduction process for 24 h. Supporting Information Figure S2 shows clearly that the color of GO suspensions changes from brown to black and the absorbance increases as well after undergoing a photothermal reduction process. Moreover, the normalized absorbance spectra of rGO with other exposure times of photothermal reduction process are also shown in Supporting Information Figure S3, suggesting no change of rGO absorb-

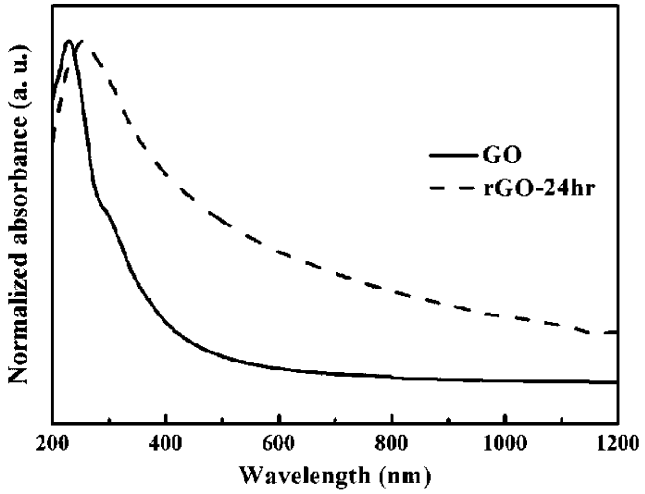

Fig. 1. The normalized absorbance spectra of suspensions with GO and photothermal reduced graphene oxide (rGO) obtained after a photothermal reduction process for 24 h.

ance after 6 h. These results confirms that GO was successfully reduced by the photothermal reduction process.

Supporting Information Figure S4 shows the photographs of GO and rGO obtained by being subjected to the photothermal reduction process with various exposure times (6 to 72 h). The color gradually changes from the original light brown to black with increasing exposure time. It can be inferred that the oxidation state of rGO is a function of the exposure time in the photothermal reduction process. In order to identify the oxidation state of rGO, Raman spectra was used to observe the degree of graphitization of rGO with various exposure times, as shown in Figure 2a. The intensity ratio of I_D/I_G can serve as an approximate index for evaluating the graphitic quality of carbon materials. The I_D/I_G value shows the decreasing trend as a function of the exposure time during the photothermal reduction process, as shown in Figure 2b. Larger value of I_D/I_G is attributed to the abundant oxygen-based functional groups attached on the surface of rGO, accompanying the decoration of heteroatoms and thus producing amorphous carbon. With the increase in the exposure time of the photothermal reduction process, oxygen functionalities gradually diminished from the surface of rGO, resulting in a lower level of oxidation state, and further leading to the decreased value of I_D/I_G. Moreover, the contact angle of water on the films of GO and rGO with various exposure times of the photothermal reduction process were obtained and shown in Figure 3. The water contact angle of the GO film is 22.4°, implying the good hydrophilic property for GO owing to its abundant oxygen-based functional groups on the surface. Also, the contact angle shows the increasing trend as a function of the exposure time during the photothermal reduction process, indicating that the removal of the oxygen-containing groups on the surface of rGO can be achieved by the photothermal reduction process, as confirmed earlier by Raman spectra as well.

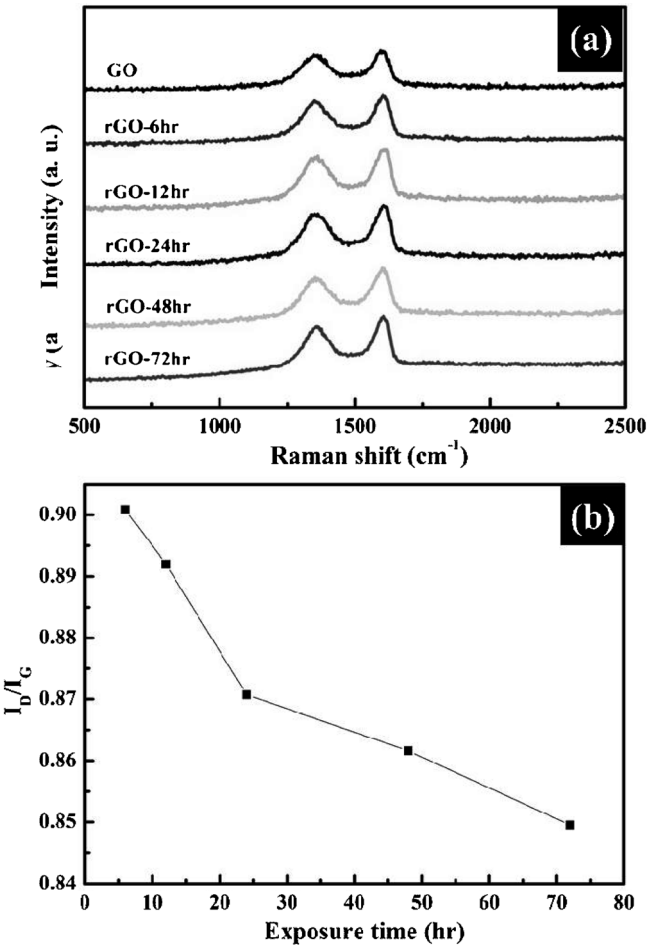

Fig. 2. (a) Raman spectra of GO and rGO under various exposure times (6 to 72 h) for the photothermal reduction process; (b) the value of I_D/I_G showing the decreasing trend as a function of the exposure time (6 to 72 h) in the photothermal reduction.

Accordingly, it can be inferred that the oxidation state of rGO is tunable by controlling the exposure time of the photothermal reduction process. Therefore, the electrocatalytic ability of rGO with various oxidation states for reducing I_3^- can be explored systematically using this method.

3.3 Cyclic Voltammetry Analysis of the Electrocatalytic Ability for I_3^- Reduction at the GO and rGO Electrodes Under Various Exposure Times

CV was performed to understand the reaction kinetics and electrocatalytic abilities of the GO and rGO electrodes with various exposure times. Figure 4 shows the CVs of the electrodes containing the GO and rGO with various exposure times, and the corresponding parameters are listed in Table 1. In a DSSC, the photoexcited electrons from the dye are injected into the TiO_2 conduction band. The oxidized dye is then reduced by the I^- in the electrolyte and the resulting I_3^- is reduced at the CE. The redox reactions at the photoanode and the CE are shown in Equation 1 and 2, respectively:

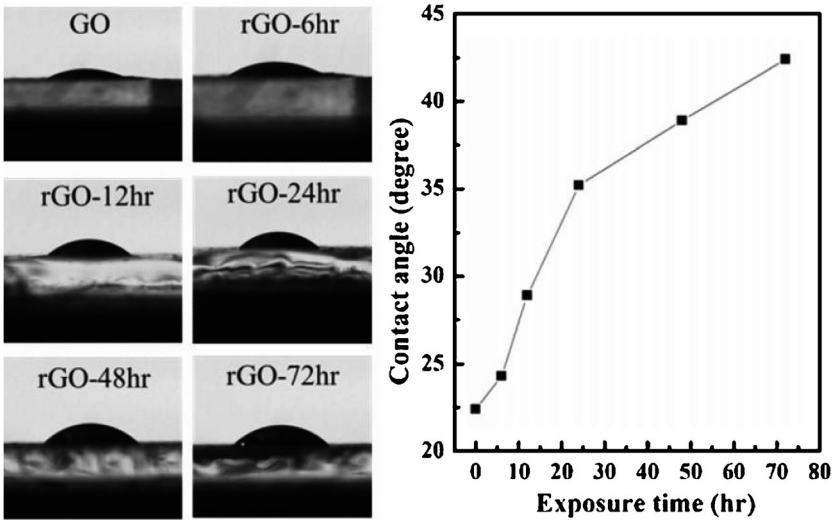

Fig. 3. Contact angle images and the trend of the contact angle value for GO and rGO under various exposure times (6 to 72 h) for the photothermal reduction process.

$$3I^- \rightarrow I_3^- + 2e^- \quad (1)$$

$$I_3^- + 2e^- \rightarrow 3I^- \quad (2)$$

It can be seen in Table 1 that the peak current densities (J_p) increase with increasing exposure time of the photothermal reduction process; this increase in the J_p is tantamount to the increase in the electrocatalytic ability of the electrodes for reducing I_3^-. The result of CV measurement indicates that diminishing the oxidation state of rGO, namely, removing oxygen-based functional groups, can efficiently facilitate the kinetics of I^-/I_3^- redox reaction, and thus inducing higher J_p value. The enhanced electrocatalytic activity of rGO electrodes with longer exposure time is certainly associated with the decreasing oxidation extent of GO and increasing active site for reducing I_3^-. This result indicates that rGO can be successfully prepared by the photothermal reduction and further used as the catalyst for catalyzing the I_3^- reduction. Moreover, the value of J_p for the electrode with rGO-72hr (4.70 mA cm^{-2}) is much higher than that of the Pt-coated electrode (2.55 mA cm^{-2}, as shown in Supporting Information Figure S5a). This suggests that rGO is a potential catalyst for replacing the conventional Pt catalyst in DSSCs.

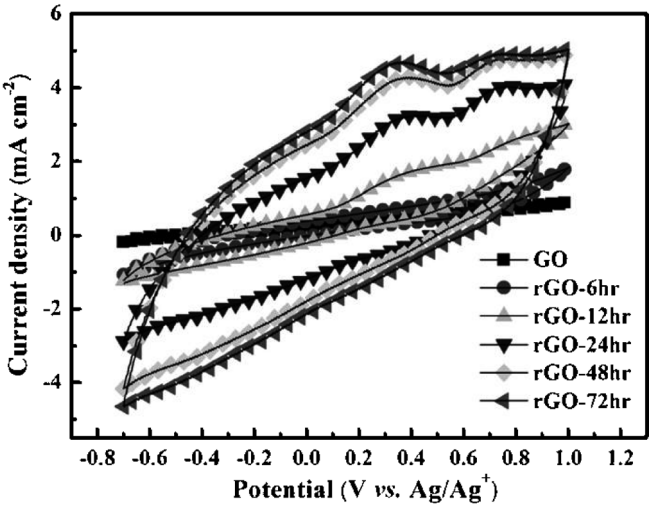

Fig. 4. Cyclic voltammograms of the electrodes with GO and rGO under various exposure times (6 to 72 h) for the photothermal reduction process, recorded in an electrolyte containing 10.0 mM LiI, 1.0 mM I_2, and 0.1 M $LiClO_4$ in ACN, at a scan rate of 100 mV s^{-1}.

Table 1. Cyclic voltammetric (CV), electrochemical impedance spectroscopic (EIS), and rotating disk electrode (RDE) data of the electrodes with GO and rGO under various exposure times (6 to 72 h) for the photothermal reduction process.

Samples	J_p (mA cm^{-2}) [a]	R_s(Ω cm^2) [b]	R_{ct} (Ω cm^2) [b]	k^0 (cm s^{-1}) [c]	A_e (cm^2 g^{-1}) [c]
GO	0.49	46.5	272.6	0.38×10^{-3}	598
rGO-6hr	0.74	22.0	51.4	0.53×10^{-3}	1483
rGO-12hr	1.64	16.0	12.1	0.62×10^{-3}	1467
rGO-24hr	3.19	16.5	7.8	0.87×10^{-3}	1576
rGO-48hr	4.27	12.4	9.3	1.08×10^{-3}	1490
rGO-72hr	4.70	11.5	4.0	2.83×10^{-3}	1372

[a] CV measurement; [b] EIS analysis; [c] RDE analysis.

Also, the result shows that the rGO exhibits a promising potential for replacing conventional Pt CEs in DSSCs. In order to further investigate the resistance of the substrate and charge transfer behaviors of the GO and rGO electrodes with various exposure times of the photothermal reduction process, electrochemical impedance spectra (EIS) and Tafel polarization analysis were performed with symmetric cells.

3.4 Electrochemical Impedance Spectra of the GO and rGO Electrodes Under Various Exposure Times

The charge transfer resistance (R_{ct}) for the reduction of I_3^- at the electrode/electrolyte interface was investigated by EIS, using a symmetric cell composed of two identical electrodes. Figure 5 shows Nyquist plots of the electrodes with GO and rGO with various exposure times of the photothermal reduction process; the equivalent circuit is shown in the figure as an inset. A Nyquist plot of a symmetric cell is associated with three parts of the impedance. The values of ohmic series resistance (R_s) of the substrate and its catalytic layer, charge transfer resistance at the interface of the electrode with the electrolyte (R_{ct}) and Warburg resistance (Z_W) in the electrolyte were evaluated by fitting the impedance spectra in the equivalent circuit, and are given in Table 1. The Nyquist plot of a symmetric cell is associated with three parts of the impedance. The result reveals that the R_s value dramatically reduced from 46.5 to 11.5 cm^2 for GO to rGO with the photothermal reduction after 72 h. It is therefore concluded that GO is gradually reduced to rGO with increasing exposure time of the photothermal reduction process, and the electric conductivity is incrementally enhanced as well. The result also indicates that the enhancement on the conductivity of rGO decreases after 12 hr, implying that most of GO would be reduced by the photothermal reduction process after half day. The value of R_{ct} is in general consistent with the electrocatalytic ability of the corresponding CEs, i.e., the value of R_{ct} would be higher with smaller value of J_p. The trend of R_{ct} values is in good agreement with the values of J_p obtained from the corresponding CV measurements. The lowest value of R_{ct} was observed for the electrode with rGO-72hr due to the high electrocatalytic activity for reducing I_3^-. It is worth mentioning that the values of R_s and R_{ct} for the electrode with rGO-72hr are close to that of the Pt-coated electrode ($R_s = 7.23$ cm^2 and $R_{ct} = 4.21$ cm^2, see related EIS data shown in Supporting Information Figure S5b), implying that rGO can be successfully prepared by the photothermal reduction process and further used as the low-cost catalyst of CEs for DSSCs.

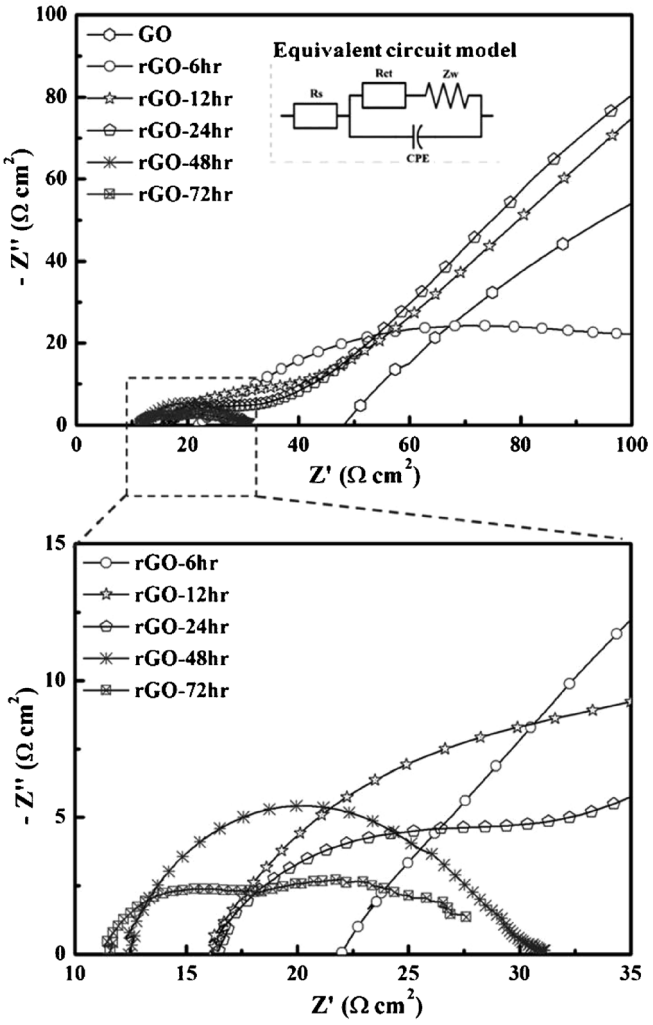

Fig. 5. Nyquist plots of the electrodes with GO and rGO under various exposure times (6 to 72 h) for the photothermal reduction process, obtained at zero bias potential; the equivalent circuit is shown in the figure as an inset.

3.5 Tafel Polarization Plots for the GO and rGO Electrodes Under Various Exposure Times

Tafel polarization analysis was performed in order to further confirm the electrocatalytic property of the GO and rGO electrodes with various exposure times of the photothermal reduction process. Figure 6 shows plots of the logarithmic current density (log J) versus the potential (V), i.e. Tafel curves, obtained with the same symmetric cell measured in EIS. Theoretically, there are three zones for each of the Tafel curves; the curve at low potentials ($|V| < 120$ mV) represents the polarization zone, the one at the middle potentials (with a sharp slope) represents the Tafel zone, and the other at the high potentials (horizontal part) represents the diffusion zone. The exchange current density (J_0) of an electrode obtained from the Tafel zone is tantamount to the electrocatalytic ability of the electrode [30b].

The value of J_0 can be estimated from the extrapolated intercepts of the anodic and cathodic branches for the corresponding Tafel curves at the current density axes. The slopes of the cathodic and anodic branches in the Tafel zone are higher for the electrode with rGO-72hr than those of GO and rGO with other exposure times, indicating the highest value of J_0 for the former case ac-

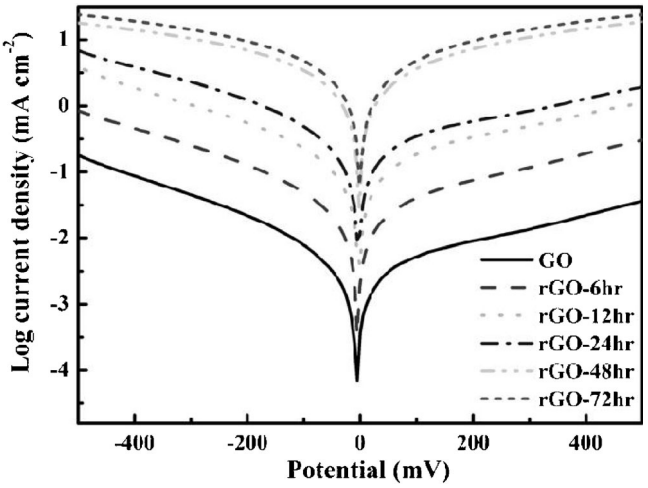

Fig. 6. Tafel polarization curves of the electrodes with GO and rGO under various exposure times (6 to 72 h) for the photothermal reduction process, obtained using a symmetrical cell with two identical electrodes.

cording to the Tafel equation [32]. The results indicate that the electrode with rGO-72hr can catalyze the reduction of I_3^- to I^- more effectively than the electrodes with the films of GO and rGO with other exposure times; this is in consistency with the highest value of J_p and the lowest value of R_{ct} of the electrode with rGO-72hr.

In addition, higher value of J_0 also implies lower value of R_{ct}. The relation between these two parameters can be expressed as follows [33],

$$J_0 = RT/nFR_{ct} \quad (3)$$

where R is the gas constant, T is the temperature, F is Faraday's constant, n is the number of electrons involved in the reduction of I_3^- to I^-, and R_{ct} is the charge transfer resistance. The trend of R_{ct} values in the Tafel polarization measurement is in consistent with the result obtained from the EIS measurement.

3.6 Rotating Disk Electrode for Determining the Electrocatalytic Abilities at the GO and rGO Electrodes Under Various Exposure Times

The catalyst layer on the CE of DSSCs should possess both a high electrocatalytic activity and a high electroactive surface area. However, CV, EIS, and Tafel polarization curves cannot distinguish these two parameters at the same time; instead, only the overall electrocatalytic ability of the CE can be extracted. Therefore, RDE was applied to determine these two parameters separately. The standard heterogeneous rate constant (k^0) and the electrocatalytic surface area (A_e) for I_3^- reduction reaction for the three electrodes with GO and rGO at various exposure times of the photothermal reduction process were estimated according to Koutecký–Levich equation [34]. The corresponding current, i, was obtained from each of the LSV curves at the formal potential (E^0 = 0.35 V vs. NHE) [35]. Therefore, the original Koutecký–Levich equation can be simplified to Equation 4. The values of k^0 and A_e were extracted by using the modified Koutecký–Levich equation, which relates the current to the rotating speed; Equation 4 can be written as follows [30a]:

$$i^{-1} = [nFA_e k^0 C_{I_3^-}]^{-1} + [0.62nFA_e D^{2/3} v^{-1/6} \omega^{1/2}\ C_{I_3^-}]^{-1} \quad (4)$$

where i is the current obtained from the LSV curves at E^0, A_e is the active surface area, k^0 is the standard heterogeneous electrochemical rate constant for I_3^- reduction reaction, $C_{I_3^-}$ is the concentration of I_3^- equal to 1.0 mM, D is the diffusion coefficient of I_3^- equal to 3.62×10^{-6} cm^{2}s^{-1}, v is the kinematic viscosity of ACN equal to 4.71×10^{-3} cm^{2}s^{-1}, and ω is the angular velocity converted from the rotating speed.

Figure 7 shows plots of i^{-1} vs. $\omega^{-1/2}$ for the RDE with thin films of GO and rGO with various exposure times. The values of k^0 and A_e for these films were respectively calculated from the intercept and the slope of the plot using Koutecký–Levich equation after fitting the data in the plots. The parameters of k^0 and A_e are listed in Table 1. GO shows smaller k^0 and A_e than those of the rGO with various exposure times; this result can be explained by the poor electric conductivity and less active site for GO with high level oxidation states. The k^0 value of rGO gradually increases with extending the exposure time of photothermal reduction process, implying that the intrinsic electrocatalytic activity for reducing I_3^- can be facilitated for the rGO with lower oxidation state. However, the A_e value of rGO gradually decreases with further increases of the exposure time from 24 to 72 h. This interesting result may be caused by aggregation of rGO with less functional group on its surface, which can be ob-

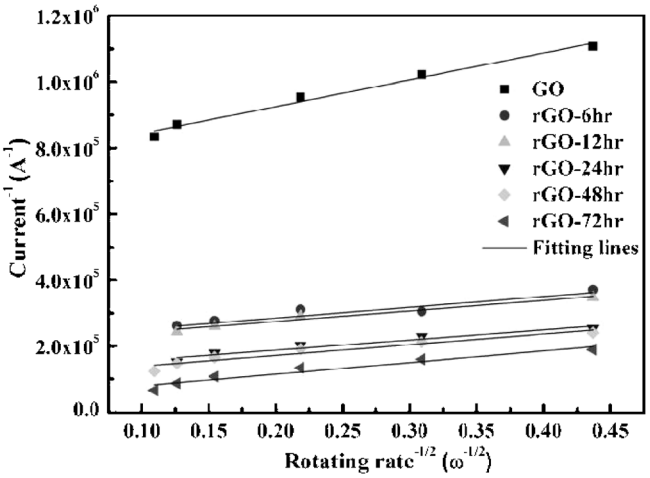

Fig. 7. Plots of i^{-1} vs. $\omega^{-0.5}$ for the RDE with the films of GO and rGO under various exposure times (6 to 72 h) for the photothermal reduction process.

served in Supporting Information Figure S4 (in the case of rGO-72 hr). The result suggests that the dominant parameter for controlling the electrocatalytic ability of rGO for reducing I_3^- is k^0 instead of A_e.

4 Conclusions

Home-made rGO with various oxidation states can be controlled by applying a modified photothermal reduction under various exposure times. With increasing the exposure time of the photothermal reduction process, oxygen functionalities gradually diminished from the surface of rGO, resulting in the lower level of oxidation state and further decreased the ratio of I_D/I_G, obtained from Ramen spectra. The J_p value of rGO obtained from CV increased with increasing photothermal reduction exposure time, indicating the facilitated kinetics of I^-/I_3^- redox reaction, due to the more reduction of rGO oxidation states by more removal of oxygen-based functional groups, and therefore the more active site on rGO for reducing I_3^-. The trend of CV is in good agreement with that obtained from the EIS analysis and Tafel polarization curve. The R_S values obtained from the EIS decreased from GO to rGO-72hr, suggesting that the GO was gradually reduced to rGO with increasing photothermal reduction exposure time, and the corresponding electric conductivity was simultaneously enhanced incrementally. Moreover, higher k^0 and A_e values measured by the RDE were obtained for rGO with various exposure times with reference to those of GO, due to the better electric conductivity and more active sites for rGO with low level oxidation states. The RDE results suggest that the dominant parameter for controlling the electrocatalytic ability of rGO for reducing I_3^- is k^0 other than A_e.

Acknowledgements

This work was supported in part by the *National Science Council* (*NSC*) of Taiwan, under Grant Numbers NSC 100-2221-E-002-242-MY2, NSC 100-3113-E-008-003, and NSC 100-2218-E-011-027. Some of the instruments used in this study were made available through the financial support of the *Academia Sinica*, Taipei, Taiwan, under Grant Number AS-100-TP-A05.

References

[1] W. Li, C. Liang, W. Zhou, J. Qiu, G. Sun, Q. Xin, *J. Phys. Chem. B* **2003**, *107*, 6292.
[2] G. Che, B. B. Lakshmi, E. R. Fisher, C. R. Martin, *Nature* **1998**, *393*, 346.
[3] A. C. Dillon, K. M. Jones, T. A. Bekkedahl, C. H. Kiang, D. S. Bethune, M. J. Heben, *Nature* **1997**, *386*, 377.
[4] K. Besteman, J.-O. Lee, F. G. M. Wiertz, H. A. Heering, C. Dekker, *Nano Lett.* **2003**, *3*, 727.
[5] Y. Zhu, S. Murali, M. D. Stoller, K. J. Ganesh, W. Cai, P. J. Ferreira, A. Pirkle, R. M. Wallace, K. A. Cychosz, M. Thommes, D. Su, E. A. Stach, R. S. Ruoff, *Science* **2011**, *332*, 1537.
[6] X. Fang, T. Ma, G. Guan, M. Akiyama, T. Kida, E. Abe, *J. Electroanal. Chem.* **2004**, *570*, 257.
[7] T. N. Murakami, M. Grätzel, *Inorg. Chim. Acta* **2008**, *361*, 572.
[8] Y.-L. Lee, C.-L. Chen, L.-W. Chong, C.-H. Chen, Y.-F. Liu, C.-F. Chi, *Electrochem. Commun.* **2010**, *12*, 1662.
[9] T.-L. Hsieh, H.-W. Chen, C.-W. Kung, C.-C. Wang, R. Vittal, K.-C. Ho, *J. Mater. Chem.* **2012**, *22*, 5550.
[10] C.-M. Chen, C.-H. Chen, T.-C. Wei, *Electrochim. Acta* **2010**, *55*, 1687.
[11] C.-Y. Lin, J.-Y. Lin, J.-L. Lan, T.-C. Wei, C.-C. Wan, *Electrochem. Solid State Lett.* **2010**, *13*, D77.
[12] K. Imoto, K. Takahashi, T. Yamaguchi, T. Komura, J. I. Nakamura, K. Murata, *Sol. Energy Mater. Sol. Cells* **2003**, *79*, 459.
[13] T. N. Murakami, S. Ito, Q. Wang, M. K. Nazeeruddin, T. Bessho, I. Cesar, P. Liska, R. Humphry-Baker, P. Comte, P. Péchy, M. Grätzel, *J. Electrochem. Soc.* **2006**, *153*, A2255.
[14] F. Cai, J. Chen, R. Xu, *Chem. Lett.* **2006**, *35*, 1266.
[15] Z. Huang, X. Liu, K. Li, D. Li, Y. Luo, H. Li, W. Song, L. Chen, Q. Meng, *Electrochem. Commun.* **2007**, *9*, 596.
[16] J. Chen, K. Li, Y. Luo, X. Guo, D. Li, M. Deng, S. Huang, Q. Meng, *Carbon* **2009**, *47*, 2704.
[17] a) T. Hino, Y. Ogawa, N. Kuramoto, *Fuller. Nanotub. Carbon Nanostruct.* **2006**, *14*, 607; b) K. Suzuki, M. Yamaguchi, M. Kumagai, S. Yanagida, *Chem. Lett.* **2003**, *32*, 28; c) E. Ramasamy, W. J. Lee, D. Y. Lee, J. S. Song, *Electrochem. Commun.* **2008**, *10*, 1087.
[18] M. Wu, X. Lin, T. Wang, J. Qiu, T. Ma, *Energy Environ. Sci.* **2011**, *4*, 2308.
[19] K. S. Novoselov, A. K. Geim, S. V. Morozov, D. Jiang, Y. Zhang, S. V. Dubonos, I. V. Grigorieva, A. A. Firsov, *Science* **2004**, *306*, 666.
[20] F. Schedin, A. K. Geim, S. V. Morozov, E. W. Hill, P. Blake, M. I. Katsnelson, K. S. Novoselov, *Nat. Mater.* **2007**, *6*, 652.
[21] E. J. Yoo, J. Kim, E. Hosono, H. S. Zhou, T. Kudo, I. Honma, *Nano Lett.* **2008**, *8*, 2277.
[22] M. D. Stoller, S. Park, Z. Yanwu, J. An, R. S. Ruoff, *Nano Lett.* **2008**, *8*, 3498.
[23] A. Peigney, C. Laurent, E. Flahaut, R. R. Bacsa, A. Rousset, *Carbon* **2001**, *39*, 507.
[24] a) X. Wang, L. Zhi, K. Müllen, *Nano Lett.* **2008**, *8*, 323; b) L. Kavan, J. H. Yum, M. Grätzel, *ACS Nano* **2010**, *5*, 165; c) J. D. Roy-Mayhew, D. J. Bozym, C. Punckt, I. A. Aksay, *ACS Nano* **2010**, *4*, 6203.
[25] a) X. Huang, X. Qi, F. Boey, H. Zhang, *Chem. Soc. Rev.* **2012**, *41*, 666; b) H. Zheng, C. Y. Neo, X. Mei, J. Qiu, J. Ouyang, *J. Mater. Chem.* **2012**, *22*, 14465.
[26] C. T. Chien, S. S. Li, W. J. Lai, Y. C. Yeh, H. A. Chen, I. S. Chen, L. C. Chen, K. H. Chen, T. Nemoto, S. Isoda, M. Chen, T. Fujita, G. Eda, H. Yamaguchi, M. Chhowalla, C. W. Chen, *Angew. Chem. Int. Ed.* **2012**, *51*, 6662.
[27] W. S. Hummers, R. E. Offeman, *Am. Chem. Soc.* **1958**, *80*, 1339.
[28] A. Hauch, A. Georg, *Electrochim. Acta* **2001**, *46*, 3457.
[29] a) L. Han, N. Koide, Y. Chiba, A. Islam, T. Mitate, *C. R. Chim* **2006**, *9*, 645; b) L. Han, N. Koide, Y. Chiba, T. Mitate, *Appl. Phys. Lett.* **2004**, *84*, 2433.
[30] a) L. R. F. Allen J. Bard, in *Electrochemical Methods: Fundamentals and Applications,* 2nd ed., Wiley, New York, **2001**, pp. 331–367; b) M. Wu, X. Lin, A. Hagfeldt, T. Ma, *Chem. Commun.* **2011**, *47*, 4535.
[31] M.-C. Hsiao, S.-H. Liao, M.-Y. Yen, C.-C. Teng, S.-H. Lee, N.-W. Pu, C.-A. Wang, Y. Sung, M.-D. Ger, C.-C. M. Ma, M.-H. Hsiao, *J. Mater. Chem.* **2010**, *20*, 8496.

[32] M. Wang, A. M. Anghel, B. Marsan, N. L. C. Ha, N. Pootrakulchote, S. M. Zakeeruddin, M. Grätzel, *J. Am. Chem. Soc.* **2009**, *131*, 15976.
[33] M. Wu, X. Lin, A. Hagfeldt, T. Ma, *Angew. Chem. Int. Ed.* **2011**, *50*, 3520.
[34] K. C. Huang, C. W. Hu, C. Y. Tseng, C. Y. Liu, M. H. Yeh, H. Y. Wei, C. C. Wang, R. Vittal, C. W. Chu, K. C. Ho, *J. Mater. Chem.* **2012**, *22*, 14727.
[35] G. Boschloo, A. Hagfeldt, *Accounts Chem. Res.* **2009**, *42*, 1819.

Received: July 5, 2013
Accepted: August 4, 2013
Published online: October 11, 2013

